Novel Zn^{2+} Coordination by the Regulatory N-Terminus Metal Binding Domain of *Arabidopsis thaliana* Zn^{2+}-ATPase HMA2†

Elif Eren, Manuel González-Guerrero, Brad M. Kaufman, and José M. Argüello*

Department of Chemistry and Biochemistry, Worcester Polytechnic Institute, Worcester, Massachusetts 01609

Received January 23, 2007; Revised Manuscript Received April 6, 2007

ABSTRACT: *Arabidopsis thaliana* HMA2 is a Zn^{2+} transporting P_{1B}-type ATPase required for maintaining plant metal homeostasis. HMA2 and all eukaryote Zn^{2+}-ATPases have unique conserved N- and C-terminal sequences that differentiate them from other P_{1B}-type ATPases. Homology modeling and structural comparison by circular dichroism indicate that the 75 amino acid long HMA2 N-terminus shares the $\beta\alpha\beta\beta\alpha$ folding present in most P_{1B}-type ATPase N-terminal metal binding domains (N-MBDs). However, the characteristic metal binding sequence CysXXCys is replaced by Cys17CysXXGlu21, a sequence present in all plant Zn^{2+}-ATPases. The isolated HMA2 N-MBD fragment binds a single Zn^{2+} (K_d 0.18 μM), Cd^{2+} (K_d 0.27 μM), or, with less affinity, Cu^+ (K_d 13 μM). Mutagenesis studies indicate that Cys17, Cys18, and Glu21 participate in Zn^{2+} and Cd^{2+} coordination, while Cys17 and Glu21, but not Cys18, are required for Cu^+ binding. Interestingly, the Glu21Cys mutation that generates a CysCysXXCys site is unable to bind Zn^{2+} or Cd^{2+} but it binds Cu^+ with affinity (K_d 1 μM) higher than wild type N-MBD. Truncated HMA2 lacking the N-MBD showed reduced ATPase activity without significant changes in metal binding to transmembrane metal binding sites. Likewise, ATPase activity of HMA2 carrying mutations Cys17Ala, Cys18Ala, and Glu21Ala/Cys was also reduced but showed a metal dependence similar to the wild type enzyme. These observations suggest that plant Zn^{2+}-ATPase N-MBDs have a folding and function similar to Cu^+-ATPase N-MBDs. However, the unique Zn^{2+} coordination via two thiols and a carboxyl group provides selective binding of the activating metals to these regulatory domains. Metal binding through these side chains, although found in different sequences, appears as a common feature of both bacterial and eukaryotic Zn^{2+}-ATPase N-MBDs.

P_{1B}-type ATPases transport transition metal ions (Ag^+, Cu^+, Cu^{2+}, Zn^{2+}, Cd^{2+}, Pb^{2+}, Co^{2+}) across biological membranes using the energy of ATP hydrolysis (*1*−*3*). Found in almost all organisms, from archaea to humans, these ATPases are key components of metal homeostasis mechanisms (*2*, *4*, *5*). Their importance is highlighted by Menkes and Wilson's diseases which are caused by mutations in the coding sequence of the two human Cu^+-ATPases (*5*, *6*). While other eukaryotes have only two Cu^+-ATPase isoforms (*1*, *3*), plants contain eight or nine genes coding for diverse P_{1B}-type ATPases, i.e., Zn^{2+}-ATPases and Cu^+-ATPases (*4*). Inhibition of these genes' expression leads to significant imbalances in Zn^{2+} and Cu^+ homeostasis (*7*−*11*). In particular, the unique presence of Zn^{2+}-ATPases in plants illustrates the distinct strategies used by these organisms for transition metal distribution and emphasizes the importance of their characterization. Biochemical studies of one of these Zn^{2+}-ATPases, *Arabidopsis thaliana* HMA2, have shown that it drives Zn^{2+} efflux out of the cell (*8*). Following the classical E1/E2 Albers-Post mechanisms, the enzyme is activated by cytoplasmic Zn^{2+} and Cd^{2+} with low apparent affinities (0.1−0.2 μM) and transports the metal upon ATP hydrolysis and formation of a phosphorylated intermediate. A number of structural features are common to plant Zn^{2+}-ATPases (*4*). Their distinct cytoplasmic N- and C-terminal sequences are of particular interest since they are likely involved in metal binding and regulation of transport (*4*, *12*, *13*).

Most P_{1B}-type ATPases have 8 transmembrane helices (TM) (*1*, *3*, *6*, *14*). Conserved residues in TMs H6, H7, and H8 form the transmembrane metal binding domain (TMBD[1]) and provide signature sequences that predict the corresponding metal specificity (*1*, *15*−*18*). The large cytoplasmic loop between TMs H6 and H7 is responsible for ATP binding and hydrolysis. This segment encompasses the nucleotide binding (N) and phosphorylation (P) domains (*19*). A smaller cytoplasmic loop located between H4 and H6 forms the actuator (A) domain (*20*). In addition to the TMBD, most P_{1B}-type ATPases have regulatory cytoplasmic metal binding domains located in the N-terminus (N-MBD), C-terminus (C-MBD), or both (*1*, *5*, *12*). Typical N-MBDs present in Cu^+-ATPases are 60−70 amino acid long domains with conserved CysXXCys sequences (*2*, *5*, *21*). The high-resolution structures of Cu^+-ATPase N-MBDs show a characteristic $\beta\alpha\beta\beta\alpha\beta$ fold (*21*−*23*). These are homologous

† This work was supported by NSF Grant MCB-0235165 (J.M.A.).

* To whom correspondence should be addressed. E-mail: arguello@wpi.edu. Phone: (508) 831-5326. Fax: (508)-831-5933.

[1] Abbreviations: C-MBD, C-terminal metal binding domain; N-MBD, N-terminal metal binding domain; TM, transmembrane helices; TMBD, transmembrane metal binding domain; ΔN-HMA2, N-terminus truncated HMA2 lacking the first 75 amino acids; TCEP, tris(2-carboxyethyl)phosphine hydrochloride; DTT, dithiothreithrol; AAS, atomic absorption spectroscopy; CD, circular dichroism.

10.1021/bi7001345 CCC: $37.00
Published on Web 06/06/2007

to well-characterized Cu^+-chaperones such as human Atox1, yeast Atx1, and bacterial CopZ (*21*, *24*, *25*). In vitro, N-MBDs bind various transition metals (Cu^+, Ag^+, Zn^{2+}, Cd^{2+}) (*26*, *27*). In vivo, N-MBDs receive Cu^+ from the corresponding chaperones via ligand exchange (*28*−*30*). Cu^+ binding to Cu^+-ATPase N-MBDs appears to regulate enzyme activity (*31*−*33*). Truncation of Cu^+-ATPase N-MBDs or removal of their metal binding capability by site-directed mutagenesis results in reduced enzyme activity with small or no changes in metal dependence for ATPase activation. Studies using model *Archaeoglobus fulgidus* Cu^+- and Cu^{2+}-ATPases CopA and CopB have shown that N-MBDs control the enzyme turnover rate by affecting the rate limiting conformational change associated with metal release/dephosphorylation (*33*, *34*). Lutsenko and co-workers have shown that Wilson's disease protein N-MBDs interact with the ATP binding domain in a Cu^+-dependent manner (*35*). Moreover, in the cases of Menkes and Wilson's disease proteins, at least one N-MBD domain is required for the targeting of these proteins to the plasma membrane and a vesicular compartment respectively (*5*, *36*, *37*).

While the N-MBDs present in Cu^+-ATPases are well-characterized, distinct N- and C-terminal sequences present in eukaryote (plant) Zn^{2+}-ATPases have received little attention (*12*, *13*, *38*). Characterization of their molecular function and in planta physiological roles is relevant since they likely regulate metal transport rate and protein targeting. Recently, we characterized the 244 amino acid long C-terminus metal binding domain (C-MBD) of *A. thaliana* Zn^{2+}-ATPase HMA2 (*12*). Truncation of the C-MBD results in ≈50% decrease in HMA2 activity without significantly altering Zn^{2+} or Cd^{2+} $K_{1/2}$ for ATPase activation. This suggests an auto stimulatory mechanism by which cytoplasmic metal binding to C-MBD drives faster transport. HMA2 C-MBD binds three Zn^{2+} with high affinity. Two of these sites coordinate Zn^{2+} with four His while the remaining site is formed by three His and a Cys. Thus, the C-MBDs present in plant Zn^{2+}-ATPases appear to have a unique architecture and consequent selectivity.

Plant Zn^{2+}-ATPases also have relatively well conserved N-termini. These approximately 70 amino acid long segments appear similar to the typical N-MBDs observed in Cu^+-ATPases and bacterial Zn^{2+}-ATPases (Figure 1). However, in plant Zn^{2+}-ATPases the metal binding CysXXCys sequence is replaced by the invariant CysCysXXGlu sequence (X = Ser, Thr, Pro, Ala), an amino acid sequence that leads to metal coordination by thiol and carboxy groups. Interestingly, the N-MBDs present in bacterial Zn^{2+}-ATPases, *Escherichia coli* ZntA and *Listeria monocytogenes* CadA, have the characteristic $\beta\alpha\beta\beta\alpha\beta$ fold and conserved CysXX-Cys sequence but contain a neighboring Asp or Glu residue that is also involved in metal binding (*39*, *40*) (Figure 1B,C). However, the relevance of these acidic residues for metal selectivity and affinity has not been tested.

This work describes the characterization of the N-MBD present in *A. thaliana* HMA2. The metal binding properties of the isolated wild type (wt) N-MBD and mutated domains carrying single replacements of residues in the Cys17CysThr-SerGlu21 sequence were determined. In addition, the Zn^{2+} dependent ATPase activities of N-terminus truncated HMA2 (ΔN-HMA2), and of HMA2s containing point mutations in the N-terminal metal binding sequence, were characterized. Findings from these experiments suggest the participation of the three conserved residues, a Glu and two Cys, in metal coordination providing a distinct selectivity to the plant Zn^{2+}-ATPase N-MBDs. As in the case of HMA2 C-MBD, metal binding to the HMA2 N-MBD controls enzyme turnover without affecting transport selectivity.

EXPERIMENTAL METHODS

Cloning and Expression of HMA2 Constructs. The yeast expression vector pYES2/CT carrying *A. thaliana* HMA2 containing a C-terminal Strep-tag (WSHPQFEK) was prepared as previously described (*12*). N-terminus truncated HMA2 (ΔN-HMA2) lacking the N-terminal first 75 amino acids, starting at Val76, and containing a C-terminal Strep-tag was amplified from a previously prepared HMA2-pPRIBA1/Strep construct by using the oligonucleotides 5′-GCGGTACCAAAAATGGTAACCGGAGAACCAA and 3′-GCGTTTAAACTTATTTTTCGAACTGC. The amplicon was ligated into the *Kpn*I and *Pme*I sites of the yeast expression vector pYES2/CT (Invitrogen, Carlsbad, CA).

Cys17Ala, Cys18Ala, Ser20Ala, Ser20Cys, Glu21Ala, and Glu21Cys HMA2 mutants were amplified using the 5′ oligonucleotides C17A, 5′-CAACGGTACCTCCGATGTA-CAAGCAATTCC; C18A, 5′-ATTTGCGCTACATCGGAG-GTACCGTTGAT; S20A, 5′-ATTTGCTGTACAGCGGAG-GTACCGTTGAT; S20C, 5′-ATTTGCTGTACATGCG-AGGTACCGTTGAT; E21A, 5′-ATTTGCTGTACATCG-GCGGTACCGTTGAT; E21C, 5′-ATTTGCTGTACTTC-GTGTGTACCGTTGAT; and the complementary 3′ primers using HMA2-pYES2/Strep as a template. The resulting linear mutant HMA2-pYES2/Strep amplicons were treated with *Dpn*I and transformed into *E. coli* TOP10 cells (Invitrogen). Sequences were verified by automated DNA sequencing (MacrogenUSA, Rockville, MD). Isolated wt and mutant HMA2 coding plasmids were then transformed into yeast strain INVSc1 *MAT*α *his3*Δ*1 leu2 trp1-289 ura3-52* (Invitrogen) by electroporation of cells at 1.5 kV, 25 μF, 200 Ω. Expression of HMA2 constructs in yeast was performed as previously described except the cells were grown in 2% Gal containing induction media for 12 h instead of 8 h (*8*).

Cloning, Expression, and Purification of HMA2 N-MBD. A cDNA coding for the first 75 amino acids of HMA2, from Met1 to Arg75, was amplified by using the oligonucleotides 5′-GCAGGTACCGCGTCGAAGAAGATG and 3′-TCGCTC-GAGCCTCACATTTGCTTCTAACTG and HMA2 cDNA as a template. The resulting amplicon was cloned into the *Kpn*I and *Xho*I sites of the bacterial expression vector pPRIBA1 (IBA, Göttingen, Germany) (N-MBD-pPRIBA1). This introduces a Strep-tag into the C-terminal end of the protein. *E. coli* BL21(DE3)pLysS cells were transformed with this vector. Cys17Ala, Cys18Ala, Ser20Ala, Ser20Cys, Glu21Ala, and Glu21Cys N-MBD mutants were amplified using the oligonucleotides listed above and N-MBD-pPRIBA1 as a template. The resulting linear N-MBD-pPRIBA1 amplicons were treated with *Dpn*I and transferred into *E. coli* BL21Star(DE3)pLysS (Invitrogen) cells. Sequences were verified by automated DNA sequencing (MacrogenUSA).

N-MBD expression was induced with 0.1 mM isopropyl-β-D-thiogalactopyranoside for 4 h. Purification of N-MBDs was performed using Strep-tag affinity chromatography, as

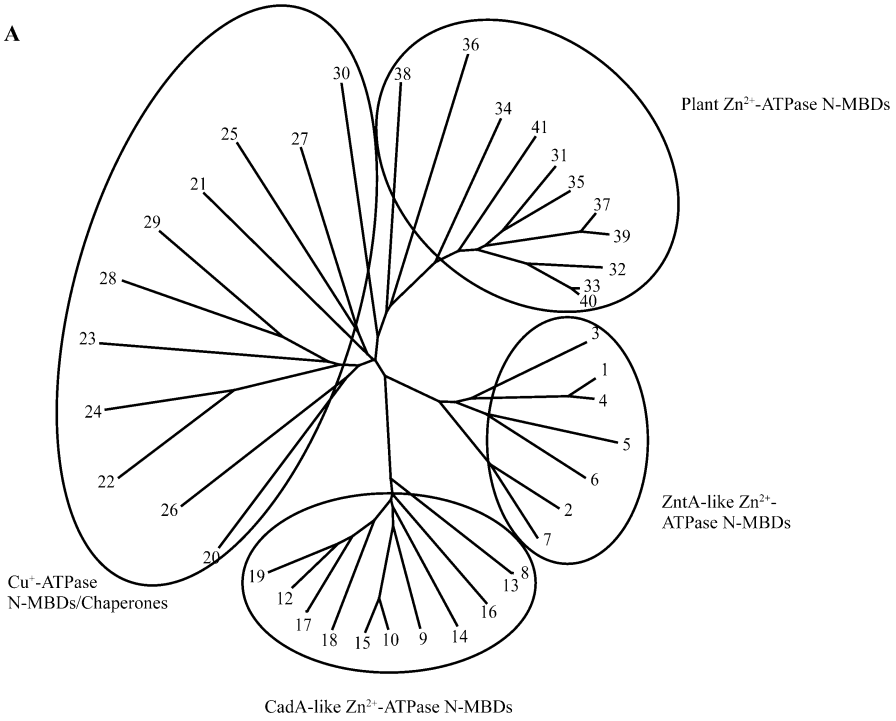

B

```
AtHMA2  Q9SZW4 MASK--------------KMTKSYFDVLGICCTSEVPLIENILNSMDGVKEFSVIVPSRT 46
MtHMA   Q1T1H3 MSSS----------EGGKKLQKSYFDVVGLCCSSEVPLIENILKPLQGVKEVSVIVPSRT 50
TcHMA4  Q70LF4 MALQKEIKNKEEDKKTKKKWQKSYFDVLGICCTSEIPLIENILKSLDGVKEYTVIVPSRT 60
AhHMA4  Q3ZDL9 MASQ----NKEEEKKKVKKLQKSYFDVLGICCTSEVPIIENILKSLDGVKEYSVIVPSRT 56
AtHMA4  O64474 MALQ----NKEEEKKKVKKLQKSYFDVLGICCTSEVPIIENILKSLDGVKEYSVIVPSRT 56
AhHMA3  Q70Q04 MAEG--------EEAKKKNLQTSYFDVVGICCTSEVSIVGDVLRPLDGVKEFSVIVPSRT 52
AtHMA3  Q9SZW5 MAEG--------EESKKMNLQTSYFDVVGICCSSEVSIVGNVLRQVDGVKEFSVIVPSRT 52
MtCof   Q1SYW8 MVEN---------------IKRSNFEVLGMCCATEATLVERILKPLHGVKAVSVIVPART 45
OsHMA3  Q0D9S9 AAEEPTRCGGGDGGGGGRKRKKTYLDVLGVCCSAEVALVERLLAPLDGVRVVSVVVASRT 81
OsHMA2  Q8H384 MAAE----------GGRCQKSYFDVLGICCPSEVPLVEKLLQPLEGVQKVTVIVPSRT 48
OtHMA   Q01EZ3 TAATIAAKLALEARGGNEPSTRTRLSVNGICCPSEVPLIHKILGKLEGVREVKVIVPTKT 63
```

C

```
StZntA  Q8ZLE5 EHCASSAPVSTAMAGT-RYTWKISGMDCAACARKVENAVRQIRGVNQAQVLFATEKLVVD  91
EcZntA  P37617 GACSSTPTLSENVSGT-RYSWKVSGMDCAACARKVENAVRQLAGVNQVQVLFATEKLVVD  91
SpZntA  A0IN11 -DEESDRLAAAPLSGSRRYSWKVTGMDCPSCAKKIENAVTALPGVDNARVLFATEKLVVD 125
YpZntA  Q74R56 -DEESDRLDTTIVSGTQRFSWQVKGMDCPSCARKIENAISGLDGVEKVKVLFTTEKLVVD 125
```

D

```
LmCadA  Q60048 ---GLSCTNCAAKFERNVKEIEGVTEAIVNFGASK-ITVTGEASIQQVEQAGAFEHLKII 66
StCadA  Q70C63 RVDGLSCTNCAGKFEKNVKNISGVTDAKVNFGAGK-ITVYGETSISQIEKAGAFENLKIS 69
SeCadA  Q8CQH7 -VDGFSCANCAGKFERNVKKIPGVEDAKVNFGASK-ISVYGEATVEELEKAGAFENLKVA 73
BhCadA  Q9KFC7 -IQGMTCAACSNRIEKGLQRMDGVQEANVNLTLERSTVVYDPEKVQPEQVIEKVEQLGYK 69
```

E

```
AfCopA  029777 MVKDTYISSASKTPPMERTVRVTGMTCAMCVKSIETAVGSLEGVEEVRVNLATETAFIRF  60
BsCopZ  032221 --------------MEQKTLQVEGMSCQHCVKAVETSVGELDGVSAVHVNLEAGKVDVSF  46
HsATP7A Q04656 SLQKIPLNVVSQPLTQETVINIDGMTCNSCVQSIEGVISKKPGVKSIRVSLANSNGTVEY 421
HsATP7B P35670 HSPGSPPRNQVQGTCSTTLIAIAGMTCASCVHSIEGMISQLEGVQQISVSLAEGTATVLY 403
```

FIGURE 1: Dendrogram of plant Zn^{2+}-ATPase N-MBDs, bacterial ZntA-like Zn^{2+}-ATPase N-MBDs, CadA-like Zn^{2+}-ATPase N-MBDs, and typical Cu^{+}-ATPase N-MBDs (A). The 60−75 amino acid N-MBD sequences were from *Yersinia pestis* Q74R56 (1); *E. coli* P37617 (2); *Serratia proteamaculans* A0IN11 (3); *Y. pseudotuberculosis* Q66FX0 (4); *Erwinia carotovora* Q6CZ01 (5); *Photorhabdus luminescens* Q7MZZ6 (6); *Salmonella enterica* Q571IQ1 (7); *Bacillus halodurans* Q9KFC7 (8); *L. monocytogenes* Q60048 (9); *Streptococcus thermophilus* Q70C63 (10); *Staphylococcus epidermis* Q8CQH7 (11); *B. pseudofirmus* P30336 (12); *B. halodurans* Q9K5Q2 (13); *Lactococcus lactis* Q0GU07 (14); *L. monocytogenes* P58414 (15); *Oceanobacillus iheyensis* Q8ETI5 (16); *Staphylococcus aureus* Q6GIX1 (17); *Streptococcus agalactiae* Q3D1P4 (18); *Stenotrophomonas maltophila* Q9JRM2 (19); *Streptococcus suis* Q301Y7 (20); *Anabaena variabilis* Q3ME37 (21); *Aspergillus fumigatus* Q4WQF3 (22); *Arabidopsis thaliana* Q9SH30 (23); *Neurospora crassa* Q7SGS2 (24); *Lactobacillus acidophilus* Q5FlK1 (25); *Archeoglobus fulgidus* O297777 (26); *B. subtilis* O32221 (27); *Homo sapiens* Q04656 (28); *H. sapiens* P35670 (29); *Helicobacter pylori* Q48271 (30); *A. thaliana* Q9SZW4 (31); *Thlaspi caerulescens* Q70LF4 (32); *A. halleri* Q3ZDL9 (33); *Medicago truncatula* Q1SYW8 (34); *M. truncatula* Q1T1H3 (35); *Oryza sativa* AP004278 (36): *A. halleri* Q70Q04 (37); *Ostreococcus tauri* Q01EZ3 (38); *A. thaliana* Q9SZW5 (39); *A. thaliana* O64474 (40); *O. sativa* Q8H384 (41). Multiple alignment of plant Zn^{2+}-ATPases N-MBDs (B), bacterial ZntA-like Zn^{2+}-ATPases N-MBDs (C), bacterial CadA-like Zn^{2+}-ATPases N-MBDs (D), and typical Cu^{+}-ATPases N-MBDs and Cu^{+}-chaperones (E). Positions of the last amino acid in the shown sequence are indicated. Conserved amino acids in the CysCysXXGlu and CysXXCys regions are indicated in bold. The conserved carboxyl residue participating in metal binding in bacterial Zn^{2+}-ATPases (C and D) is also highlighted in bold. Accession numbers for the different proteins are indicated after the name.

previously described for the C-MBD of HMA2 (*12*). Purified proteins were concentrated to 2 mg mL^{-1} using an Amicon Ultra-15 Centricon (Millipore, Billerica, MA) and stored in 100 mM Tris, pH 8.00, 150 mM NaCl, and 1 mM Tris(2-

carboxyethyl)phosphine hydrochloride (TCEP) at −80 °C. Protein concentration determinations were performed in accordance to Bradford (*41*) using bovine serum albumin as a standard.

Yeast Membrane Preparation. Membranes from HMA2 expressing yeasts were prepared as previously described with slight modifications in cell disruption (*8*, *12*). Briefly, the cells were disrupted in a bead beater (BioSpec, Bartlesville, OK) with 8 × 30 s homogenization with 30 s intervals using 10 mL of 0.5 mm glass beads and 15 mL cells in 10 mM Tris (pH 7.4), 250 mM Suc, 10 mM ascorbic acid, 1 mM phenylmethylsulfonyl fluoride, 1 μg mL^{-1} leupeptin, and 1 μg mL^{-1} aprotinin. SDS−PAGE was carried out in 10% acrylamide gels (*42*). Heterologous proteins in the membrane preparations were detected by electroblotting the gels onto nitrocellulose membranes and immunostaining with Strep-Tactin horseradish peroxidase antibody (IBA). The relative expression level of each protein was evaluated as previously described (*12*, *34*). Briefly, equal amounts of each membrane preparation were subjected to a 1:2 serial dilution. These were blotted onto a nitrocellulose membrane and immunostained, and integrated density values were quantified using AlphaImager software (Alpha Innotech Corp., San Leandro, CA).

ATPase Assays. Zn^{2+} dependent ATPase activity determinations were performed as previously described (*8*, *12*). The assay media contained 50 mM Tris, pH 7.5, 3 mM $MgCl_2$, 3 mM ATP, 20 mM cysteine, 1 mM dithiothreithrol (DTT), 0.01% *n*-dodecyl-β-D-maltopyranoside (DDM), and 40 μg mL^{-1} protein (membrane preparation). The concentrations of $ZnCl_2$ were varied as indicated in Figure 5. The reaction was incubated 10 min at 30 °C and inorganic phosphate determined in accordance to Lanzetta et al. (*43*). ATPase activity measured in the absence of metal was always <10% of V_{max} and was subtracted from plotted values. Curves of ATPase activity vs Zn^{2+} concentration were fit to $v = V_{max}[Zn^{2+}]/([Zn^{2+}] + K_{1/2})$. The reported standard errors for V_{max} and $K_{1/2}$ are asymptotic standard errors reported by the fitting software (Kaleidagraph, Synergy, Reading, PA). Plotted data points are the mean ± SE of at least three experiments performed with independent membrane preparations.

Characterization of Metal Binding Stoichiometry and Metal Affinity of Wild Type and Mutant N-MBDs. Total metal binding capacity was measured by atomic absorption spectroscopy (AAS) (AAnalyst 300, Perkin-Elmer, Foster City, CA) as previously described (*8*). Briefly, 100 μM wt or mutant N-MBDs in 20 mM HEPES, pH 7.0, 150 mM NaCl, 1 mM TCEP were incubated with 1.0 mM of indicated metals at 4 °C for 30 min. Replacement of TCEP with ascorbic acid had no effect on the observed result. TCEP was not included in the media in the case of Cu^{2+} binding determinations. Excess metal and TCEP was removed by passage through a Sephadex G-10 column (Sigma, St Louis, MO), and samples were digested by incubation in concentrated HNO_3 for 1 h at 80 °C and then overnight at room temperature. After digestion, 1.5% H_2O_2 was added to the samples. Background metal levels in blank samples lacking metals or protein the were <10% of those detected in metal−N-MBD samples.

N-MBD Zn^{2+} and Cd^{2+} binding affinities were determined by metal titrations of N-MBDs in the presence of mag-fura-2 (Molecular Probes, Eugene, OR) (*44*). 10 μM protein was titrated with 1 mM Zn^{2+} or Cd^{2+} in the presence of 20 μM mag-fura-2 in 10 mM BisTris, pH 7.0, 1 mM TCEP buffer, and the absorbance change at 366 nm was monitored. Free metal concentrations were calculated from $K_I = [I.Me^{2+}]/[I_{free}][Me^{2+}]$, where I is mag-fura-2, Me is the metal ion, and K_I is the association constant of mag-fura-2 for each metal. An extinction coefficient of 29900 M^{-1} cm^{-1} at 366 nm for metal-free mag-fura-2 and K_I of 8.0 × 10^6 M^{-1} for Zn^{2+} and 3 × 10^7 M^{-1} for Cd^{2+} were used in determinations of free mag-fura-2 and free metal levels (*44*). The metal−protein K_d and the number of metal binding sites (*n*) in N-MBD were calculated from $\nu = n[metal]_f/K_d(1 + ([metal]_f/K_d))$, where ν is the molar ratio of metal bound to protein (*45*). As above, reported errors for K_d and *n* are asymptotic standard errors provided by the fitting software (Origin, OriginLab, Northampton, MA). Plotted data points are the mean ± SE of at least three experiments performed with independent protein preparations.

N-MBD Cu^+ binding affinities were determined by monitoring the changes in N-MBD intrinsic fluorescence during metal titrations. Metal titrations were carried out in 10 mM BisTris, pH 7.0 containing either 1 mM TCEP or 10 mM ascorbic acid. The reaction was incubated for 2 min to reach equilibrium. Intrinsic tyrosine fluorescence was measured after excitation at 290 nm. Fluorescence intensities were measured at the maximum of the spectra (295 nm), which were scanned from 280 to 400 nm. The data were fit to $(F - F_0)/(F_{max} - F_0) = [metal]/(K_d + [metal])$, where F_0 is the fluorescence in the absence of metal, F_{max} is the fluorescence obtained at saturating metal concentrations, and *F* is the fluorescence at each metal concentration. Titration of buffer alone (10 mM BisTris, pH 7.0 containing either 1 mM TCEP or 10 mM ascorbic acid) with either Zn or Cu did not result in significant changes (<2%) in the background.

Circular Dichroism Spectroscopy. Wild type and mutant N-MBDs were passed through a Sephadex-G-10 column (Sigma) equilibrated with 20 mM phosphate, pH 7.5, 100 mM NaF, and 1 mM TCEP. Proteins were diluted to a 10 μM concentration and placed in a 1 mm quartz cuvette. Circular dichroism (CD) data were recorded on an Aviv 60DS spectrometer with a 25 nm bandwidth, and data were collected every 1 nm at 25 °C. Background spectra obtained with buffer alone were subtracted from all recorded spectra. The data were analyzed in the Dichroweb site (http://www.cryst.bbk.ac.uk/cdweb/html/home.html) using K2d analysis algorithm (*46*−*48*).

Multiple Alignment and Homology Modeling of HMA2 N-MBD. N-MBD sequence comparison was performed by means of CLUSTALW (*49*). The resulting guide tree was visualized with TreeView (*50*). A suitable template for homology modeling of HMA2 N-MBD, *Helicobacter pylori* CopZ 1yg0, was identified by performing a Fasta search (*51*) in the Protein Data Bank repository of protein structures. HMA2 N-MBD structures were modeled using SWISS-MODEL (*52*, *53*) and were visualized with PyMol (Delano Scientific, Palo Alto, CA).

RESULTS

Zn^{2+}-ATPases have been identified in a number of plants including *A. thaliana*, *A. halleri*, *Oryza sativa*, *Thlaspi*

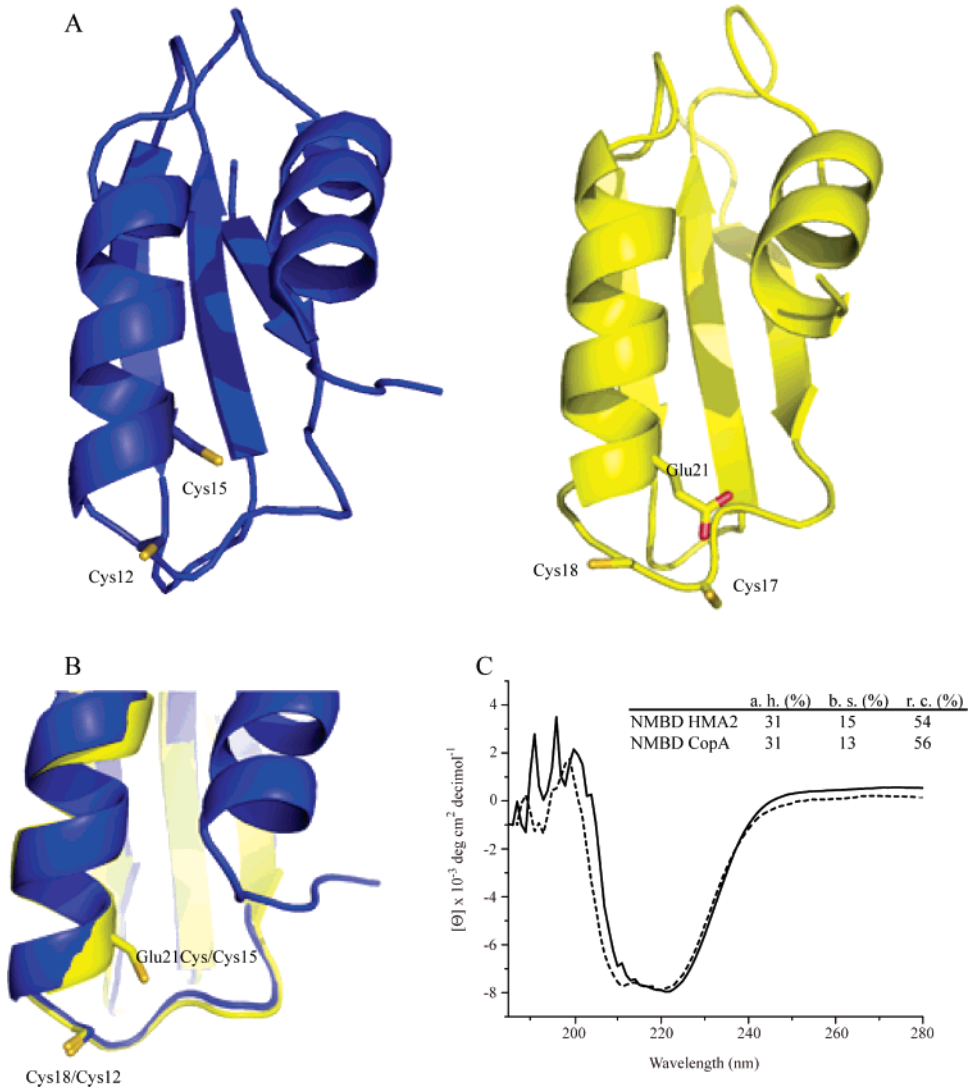

FIGURE 2: Structural aspects of HMA2 N-MBD. (A) Homology modeling of HMA2 N-MBD (right) using the structure of *Helicobacter pylori* CopZ (1yg0) as template (left). Amino acids relevant to metal binding are indicated in both structures. (B*)* Superposition of the metal binding region of 1yg0 and the Glu21Cys mutated N-MBD. The coincidence of Cys residues is indicated. (C) Circular dichroism analysis of N-MBD (—) and N-MBD of *A. fulgidus* CopA (- - -). Secondary structure elements are indicated in the inset. a. h., α-helix; b. s., *β*-sheet; and r. c., random coil. The values are given in percentages.

caerulescens, *Zea mays*, and *Sorghum bicolor* (*4*). Sequence alignment of plant Zn^{2+}-ATPase N-termini shows that these share significant homology (50−80%**)** (Figure 1A, B). Based on the higher sequence homology of the entire Zn^{2+}-ATPases with bacterial Zn^{2+}/Cd^{2+}-ATPases (34−41%) compared to the bacterial Cu^{+}-ATPases (23−36%) we expected a high similarity of these domains to either type of bacterial Zn^{2+}-ATPase N-MBDs, ZntA-like and CadA-like (*39*, *40*). However, plant Zn^{2+}-ATPase N-termini appear quite different from their bacterial homologues (homology <21%). Plant Zn^{2+}-ATPase N-termini appear to form another cluster of N-MBDs that is closer to the well-characterized Cu^{+} chaperones and Cu^{+}-ATPase N-MBDs (25−35% homology). This unexpected observation is well described by a dendrogram based only in the 60−70 amino acid sequences of the N-MBD domains (Figure 1A). Distinct from these subgroups, plant Zn^{2+}-ATPase N-termini lack the characteristic metal binding CysXXCys sequence (Figure 1B−D). Instead, they contain invariant CysCysXXGlu sequences (X = Ser, Thr, Pro, or Ala) (Figure 1B). This suggests that plant Zn^{2+}-ATPases, conserving the folding of other P_{1B}-type ATPase N-MBDs, might have developed a distinct metal coordination perhaps better suited to bind their physiological substrate.

The probable folding of HMA2 N-terminus and the structural location of its putative metal binding sequence were explored by homology modeling (Figure 2A). The Cu^{+}-chaperone from *Helicobacter pylori*, CopZ, was identified as the protein of known structure (1yg0) with the highest degree of identity (32%) with HMA2 N-MBD. The modeling of HMA2 N-MBD adopting the *β*α*ββ*α fold of *H. pylori* CopZ reported quality parameters (−3 < structure *Z*-scores < −1 and 0.6 > rms *Z*-scores > 1.7) in agreement with a good fitting to the template structure (*54*, *55*). The model shows that the CysXXCys and CysCysXXGlu motifs coincide when both structures are overlapped (Cys12 and Cys15 of *H. pylori* CopZ, with Cys18 and Glu21 of HMA2 N-MBD) (Figure 2A, B). Consequently the Cys17CysThrSerGlu21 region appears solvent accessible and arranged to receive metal from the media or from a hypothetical partner molecule via ligand exchange. The similarities among these metal binding sites are further highlighted when Glu21 is changed to Cys. In this situation, the predicted structure of

Table 1: HMA2 N-MBD Metal Binding Stoichiometry Determination by AAS

	metal bound/N-MBD				
	Zn^{2+}	Cd^{2+}	Co^{2+}	Cu^{+}	Cu^{2+}
N-MBD	0.99 ± 0.10[a]	1.20 ± 0.21	0.01 ± 0.01	1.03 ± 0.15	0.14 ± 0.01
Cys17Ala	nd[b]	0.15 ± 0.03	0.1 ± 0.04	0.16 ± 0.07	0.15 ± 0.08
Cys18Ala	0.21 ± 0.05	0.16 ± 0.05	nd	0.93 ± 0.15	0.12 ± 0.05
Ser20Ala	1.05 ± 0.07	1.20 ± 0.10	0.23 ± 0.05	1.04 ± 0.20	0.11 ± 0.01
Ser20Cys	0.83 ± 0.15	1.08 ± 0.13	nd	1.04 ± 0.23	0.04 ± 0.01
Glu21Ala	nd	0.09 ± 0.02	0.17 ± 0.06	0.25 ± 0.06	nd
Glu21Cys	0.2 ± 0.01	nd	0.20 ± 0.03	1.00 ± 0.32	0.23 ± 0.20

[a] Values are the mean $\pm$ SE ($n = 3$). [b] Not detected (under background levels).

HMA2 N-MBD mimics that of CopZ Cu^{+}-binding site (Figure 2B). To further validate this model, comparative CD analysis was performed. HMA2 N-MBD (amino acids 1 to 75) was expressed in *E. coli* and purified by affinity chromatography ($\approx$ 90% purity, data not shown). Its CD spectrum was compared to that of *A. fulgidus* CopA N-MBD. CopA is a typical Cu^{+}-ATPase, and the role of Cu^{+} binding to its N-MBD has been established (*33*, *56*). Supporting the molecular modeling, both protein fragments yielded almost identical spectra resulting from a similar secondary structure (Figure 2C).

Metal Binding to N-MBD. The functional role of HMA2 N-MBD is likely defined by its selectivity and affinity for the ATPase activating metals. In turn, these characteristics are established by the particular residues involved in the metal coordination. In order to identify these functional determinants, metal binding to isolated wt N-MBD and N-MBD carrying point mutations Cys17Ala, Cys18Ala, Ser20Ala, Ser20Cys, Glu21Ala, and Glu21Cys was measured. CD analysis showed that the substitutions have no significant effect on the N-MBD secondary structure (data not shown). Table 1 shows that wt N-MBD binds Zn^{2+} and Cd^{2+} with a stoichiometry of one metal/N-MBD. Interestingly, wt N-MBD also binds Cu^{+} (measured in the presence of TCEP), but not Cu^{2+} or Co^{2+}. N-MBDs carrying mutations Cys17Ala, Cys18Ala, or Glu21Ala did not bind Zn^{2+} or Cd^{2+}. Keeping in mind that these determinations were performed at saturating (1 mM) metal, >1000 times over the metal−N-MBD K_d (see below Table 2), the lack of binding indicates the likely participation of these side chains in the coordination of these metals. Analysis of metal binding to the Glu21Cys N-MBD revealed that, among the binding ligands, an oxygen atom seems to be essential. This mutant, although able to bind Cu^{+}, could not bind Zn^{2+} or Cd^{2+} (at least with an affinity to be detected in our experimental setting). Considering Cu^{+} binding by the N-MBD, results showed that Cu^{+} coordination appears different from that of Zn^{2+} and Cd^{2+}. While Cys17Ala and Glu21Ala mutants were unable to bind Cu^{+}, the Cys18Ala mutation did not affect Cu^{+}−N-MBD interaction, suggesting Cu^{+} coordination by Cys17 and Glu21 in the wt HMA2 N-MBD. Conversely, the Glu21Cys mutant was able to bind Cu^{+}, although in this case likely via Cys18 as proposed in Figure 2B. Finally, as expected from the sequence variability in the Ser20 position (Figure 1A), replacements Ser20Ala and Ser20Cys had no significant effects on N-MBD metal binding stoichiometry (Table 1). Thus, the described alterations in metal binding are not due to unspecific structural perturbation introduced by mutations in the region.

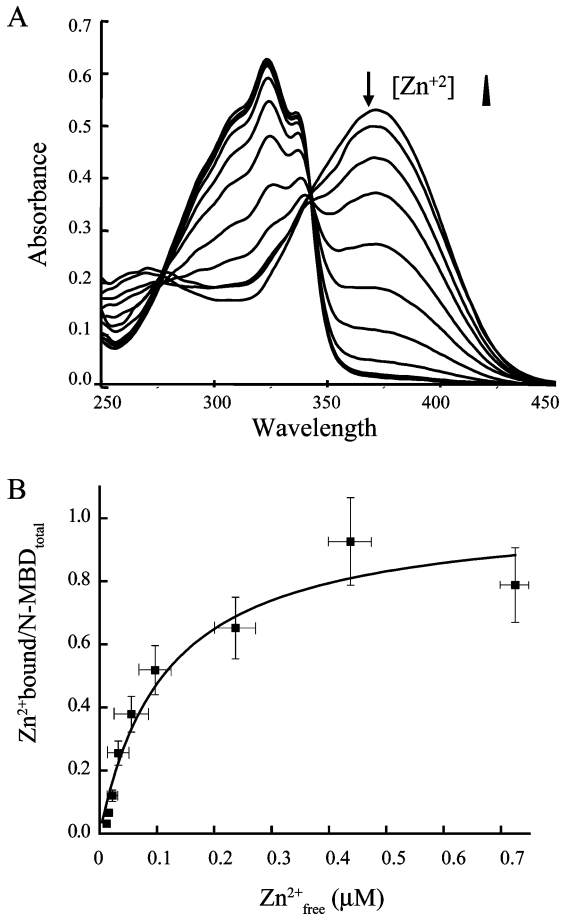

FIGURE 3: Zn^{2+} binding to wt N-MBD. (A) Representative mag-fura-2 spectra in the presence of N-MBD and increasing Zn^{2+} concentrations. The arrow shows the decrease in $OD_{366\ nm}$ with increasing Zn^{2+} concentrations. (B) Determination of wt N-MBD K_d for Zn^{2+}. The data were fitted using $n = 0.97 \pm 0.08$ and $K_d = 0.18 \pm 0.05$ μM. Values are the mean $\pm$ SE ($n = 3$).

N-MBD affinities for Zn^{2+} and Cd^{2+} were determined by titration of the isolated domain in the presence of fluorescence indicator mag-fura-2. In these experiments, mag-fura-2 forms 1:1 indicator/metal complexes of known K_d and the concentration of free indicator can be spectrophotometrically monitored (*57*). This allows the calculation of free metal and metal−protein complex levels in the system. Figure 3A and Figure 3B show the titration of wt N-MBD with Zn^{2+} in the presence of mag-fura-2. The analysis indicates that the domain binds the metal with high affinity (K_d 0.18 μM). This is comparable to the $K_{1/2}$ for Zn^{2+} activation of ATPase activity, a parameter associated with metal binding to the TMBD (*8*). Similarly, HMA2 N-MBD has high affinity for Cd^{2+} (Table 2). As expected, no divalent metal binding to Cys17Ala, Cys18Ala, Glu21Ala, and Glu21Cys mutated N-MBDs was apparent in these experiments (Table 2). The affinities of Ser20Ala or Ser20Cys mutants for Zn^{2+} or Cd^{2+} do not significantly differ from those of wt N-MBD, again suggesting that this residue does not participate in metal binding (Table 2). In our measurements we have considered the possible coordination of Zn^{2+} by the reducing agent TCEP. We measured the affinity of TCEP for Zn^{2+} and Cd^{2+} through a competitive metal titration assay using mag-fura-2 as the metal indicator. Our results showed that TCEP has a K_a of 2.3×10^3 and 1.7×10^3 for Zn^{2+} and Cd^{2+} respectively in 10 mM BisTris, pH 7.0 buffer. Therefore we concluded

Table 2: HMA2 N-MBD Zn^{2+} and Cd^{2+} K_d and Binding Stoichiometry Estimated by Mag-fura-2 Titration

	Zn^{2+}		Cd^{2+}	
	n	K_d (μM)[a]	*n*	K_d (μM)
N-MBD	0.97 ± 0.08[b]	0.18 ± 0.05	1.00 ± 0.12	0.27 ± 0.07
Cys17Ala	nd[c]	nd	nd	nd
Cys18Ala	nd	nd	nd	nd
Ser20Ala	0.93 ± 0.14	0.20 ± 0.05	0.72 ± 0.18	0.18 ± 0.06
Ser20Cys	0.75 ± 0.08	0.20 ± 0.07	1.02 ± 0.10	0.12 ± 0.03
Glu21Ala	nd	nd	nd	nd
Glu21Cys	nd	nd	nd	nd

[a] Parameters are those obtained by fitting the titration of N-MBD and mag-fura-2 with increasing Zn^{2+} or Cd^{2+} as shown in Figure 3. [b] Values are the mean ± SE ($n = 3$). [c] Not detected (under background levels).

Table 3: HMA2 N-MBD Zn^{2+} and Cu^{+} K_d Estimated by Intrinsic Fluorescence Measurements

	K_d (μM)[a]	
	Zn^{2+}	Cu^{+}
N-MBD	1.02 ± 0.31	13.89 ± 3.68
Glu21Cys	nd[b]	1.22 ± 0.59

[a] Values are the mean ± SE ($n = 3$). [b] Not detected (under background levels).

that the affect of TCEP on metal binding to HMA2 N-MBD was not significant (resulting in a 3−5% change in K_a of HMA N-MBD for Zn^{2+} or Cd^{2+}).

Cu^{+} binding to the N-MBD was monitored by changes in the intrinsic fluorescence of the purified protein. HMA2 N-MBD presents a Tyr residue (Tyr10) proximal to the metal binding site (Figure 1A). Although the conformational change within the N-MBD associated with metal binding might be relatively small (*40*), this influences Tyr10 such as changes in its fluorescence report the metal binding. Figure 4 shows the binding of Cu^{+} and Zn^{2+} to N-MBD as detected using this approach. Wt N-MBD can bind both Cu^{+} and Zn^{2+}, showing a clear preference for binding Zn^{2+} with approximately ten times more affinity (Table 3). A lower affinity of HMA2 N-MBD for Zn^{2+} was obtained measuring changes in the intrinsic fluorescence as compared with that observed by titration in the presence of mag-fura-2 (Tables 2 and 3). This apparent difference is likely associated with the parallel equilibrium of metal−mag-fura-2 system and intrinsic errors in each method. In relation to Cu^{+} binding to HMA2 N-MBD, it was shown above that the Glu21Cys mutant can bind Cu^{+} (Table 1). However, this likely occurs through Cys17 and Glu21 in the wt N-MBD and Cys18 and Glu21Cys in the mutant protein mimicking the CysXXCys site in Cu^{+}-ATPases. Supporting this alternative coordination are the different affinities for Cu^{+} that were observed in these proteins. It was determined that Glu21Cys N-MBD binds Cu^{+} with 10-fold higher affinity than the wt N-MBD (Figure 4). It is arguable then that this higher affinity is associated with removal of the carboxyl, introduction of the thiol, or better coordination geometry.

Effect of N-MBD Truncation and Mutation of Conserved Residues on HMA2 ATPase Activity. Previous studies have shown significant functional effects of metal binding to N- and C-MBDs present in P_{1B}-type ATPases (*12*, *31*−*33*, *35*, *58*, *59*). To assess the functional role of HMA2 N-MBD, the Zn^{2+}-dependent ATPase activity of HMA2, ΔN-HMA2

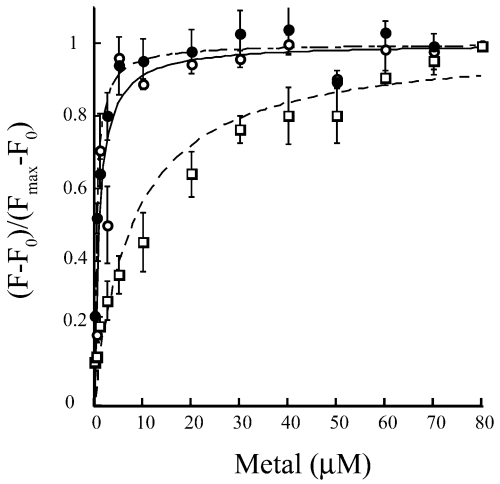

FIGURE 4: Determination of K_d of metal binding to N-MBD. N-MBD was titrated with Zn^{2+} (●) or Cu^{+} (□), and the changes in the intrinsic tyrosine fluorescence were monitored. Similarly, Glu21Cys substituted N-MBD was titrated with Cu^{+} (○). Fitting parameters are reported in Table 3. $F_{max}/F_0 = 2.4-2.8$. Values are the mean ± SE ($n = 3$).

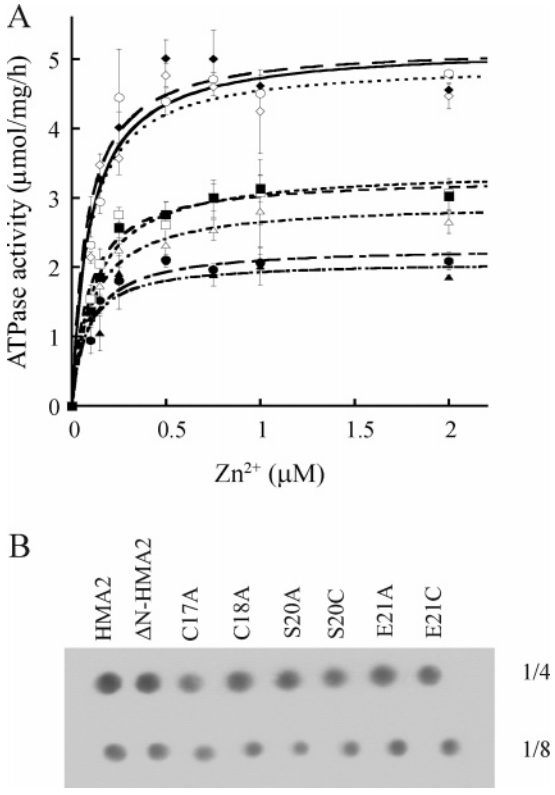

FIGURE 5: Expression and ATPase activity of HMA2, ΔN-HMA2, and N-MBD mutated HMA2. (A) Zn^{+2} dependent ATPase activity of wt HMA2 (○), ΔN-HMA2 (●), and Cys17Ala (□), Cys18Ala (■), Ser20Ala (◇), Ser20Cys (◆), Glu21Ala (△), and Glu21Cys (▲) mutants. Values are the mean ± SE ($n = 3$) normalized to relative protein expression levels. Fitting parameters are listed in Table 3. (B) Expression levels of wt HMA2 and various constructs. Dot immunoblots of two dilutions of each protein preparation are shown.

(lacking the N-MBD), and various mutated HMA2 was measured. Truncation of N-MBD resulted in a 56% decrease in V_{max} without significant changes in its metal dependence (Figure 5A and Table 4). A similar decrease of V_{max} (36−60%) was also observed in the ATPase activities of HMA2 carrying the individual mutations Cys17Ala, Cys18Ala,

Table 4: Kinetic Parameters of Wt HMA2, ΔN-HMA2, and Mutated HMA2 Zn^{2+} Dependent ATPase Activity[a]

	$K_{1/2}$ (μM)	V_{max} (μmol/mg/h)
HMA2	0.10 ± 0.02	5.18 ± 0.27
ΔN-HMA2	0.09 ± 0.02	2.29 ± 0.12
Cys17Ala	0.09 ± 0.02	3.30 ± 0.14
Cys18Ala	0.12 ± 0.02	3.41 ± 0.13
Ser20Ala	0.09 ± 0.03	4.94 ± 0.30
Ser20Cys	0.08 ± 0.02	5.19 ± 0.24
Glu21Ala	0.11 ± 0.02	2.93 ± 0.11
Glu21Cys	0.08 ± 0.03	2.08 ± 0.17

[a] Values are the mean ± SE ($n = 3$).

Glu21Ala, and Glu21Cys. On the other hand, both Ser20Ala and Ser20Cys mutants showed V_{max} similar to that of wt HMA2 (Figure 5A and Table 4). It is relevant that no significant change in metal $K_{1/2}$ for ATPase activation was detected in any of the HMA2 mutants, suggesting that N-MBD controls enzyme velocity without affecting metal binding to the TMBD (Table 4).

We have previously shown that Cu^+ (as well as various divalent transition metals) can activate HMA2 ATPase activity (Cu^+ dependent ATPase activity is 40% of that measured in the presence of Zn^{2+}) (*8*). Similar relations were observed among the Cu^+-dependent and Zn^{2+}-dependent activities of wild type protein and enzymes carrying mutations Cys18Ala and Glu21Ala (data not shown).

DISCUSSION

Most P_{1B}-type ATPases have cytoplasmic metal binding domains in their N- and/or C-termini that regulate enzyme activity (*5*, *12*, *31*−*34*, *58*, *59*). Cu^+-ATPases and most bacterial Zn^{2+}-ATPases have 60 to 70 amino acid long N-MBDs that are characterized by a $\beta\alpha\beta\beta\alpha\beta$ fold and the CysXXCys signature sequence. The thiol groups of both conserved Cys participate in metal coordination (*22*, *23*, *27*, *60*, *61*). On the other hand all eukaryote (plant) Zn^{2+}-ATPases possess a unique conserved CysCysXXGlu sequence in their N-termini that appears to provide a novel metal coordination environment. Toward understanding the function of plant Zn^{2+}-ATPase N-termini, we investigated HMA2 N-terminus metal binding capabilities, the involvement of conserved residues in metal coordination, and its role in the enzyme ATPase activity.

Metal Binding Capability of N-MBD. AAS analysis and metal titration studies showed that HMA2 N-MBD can bind Zn^{2+} and Cd^{2+} with a stoichiometry of one metal per N-MBD. It was also observed that under saturating conditions HMA2 N-MBD binds one Cu^+. This is not surprising since Cu^+-ATPase N-MBDs and Cu^+-chaperones bind a variety of non-substrate metal ions (Cu^{2+}, Zn^{2+}, Cd^{2+}, Co^{2+}, Hg^{2+}, etc.) (*26*, *27*, *29*, *62*). However, HMA2 N-MBD has ten times higher affinity for Zn^{2+} and Cd^{2+} compared to that for Cu^+. Consequently, although binding metals with relatively low affinity (compared to $<10^{-10}$ M affinities described for Cu^+-ATPases and Cu^+-chaperones) (*63*−*66*), HMA2 N-MBD can differentiate its activating metals (Zn^{2+} and Cd^{2+}) from relatively similar divalent transition metals (Co^{2+} and Cu^{2+}) and monovalent Cu^+.

HMA2 N-MBD binds Zn^{2+} and Cd^{2+} with quite similar affinities in the submicromolar range (Table 2). This is distinct from the observed metal dependence of HMA2 ATPase activity and associated transport. In this case, HMA2 appears to interact with Cd^{2+} with 3−4-fold higher affinity than for Zn^{2+} (*8*). This difference is in agreement with the idea that metal binding to the TMBD required for ATPase and transport activities is independent of metal binding to regulatory N-MBDs (*12*, *31*, *33*). On the other hand, the K_d of metal−N-MBD in HMA2 appear higher than those observed for *E. coli* ZntA N-MBD using similar determination methods (compare HMA2 $K_d = 0.18$ μM with ZntA $K_d = 0.025$ μM for the Zn^{2+}−N-MBD complex) (*44*). These dissimilarities are likely associated with the structural differences of their metal binding sites. As discussed below, although these are constituted by two thiols and a carboxyl in both enzymes, the coordinating amino acids are distinctively arranged.

Structural Characteristics of HMA2 N-MBD. The sequence similarity, good fit obtained in the homology modeling, and the CD analysis strongly support the idea that HMA2 N-MBD shares the $\beta\alpha\beta\beta\alpha$ structure of other N-MBDs including those from bacterial Zn^{2+}-ATPases (*23*, *25*, *40*). This modeling also showed that the arrangement of metal binding sequences CysCysXXGlu within HMA2 N-MBD is similar to that of CysXXCys present in the homologous domains of other P_{1B}-type ATPases and Cu^+-chaperones. Thus, although they might bind various specific metals or receive them from alternative metal trafficking molecules (no Zn^{2+} chaperone has been identified), similar structural−functional roles might be expected for all N-MBDs. That is, they might control enzyme turnover through similar intramolecular domain−domain interactions driven by metal binding.

The described results indicate that plant Zn^{2+}-ATPases N-MBDs coordinate both, Zn^{2+} and Cd^{2+}, with two conserved Cys and a Glu. Considering the homologous bacterial Zn^{2+}-ATPases, Banci and co-workers have shown that even though most of these proteins have the conserved CysXXCys sequences in their N-MBD, metal coordination is likely accomplished with the participation of a carboxyl group from an Asp or a Glu residue (*39*, *40*). In a group of bacterial Zn^{2+}-ATPases that includes *E. coli* ZntA, the metal coordinating Asp residue is located prior to the conserved Cys residues (AspCysXXCys) (*40*). Alternatively, a subset including *L. monocytogenes* CadA employs a conserved Glu located between the α-helix 2 and β-sheet 4 of their N-MBD to coordinate Cd^{2+} together with the two thiols in the CysXXCys sequence (*39*). It is apparent that plant Zn^{2+}-ATPase N-MBDs have developed an alternative strategy (i.e., amino acid sequence) to accomplish Zn^{2+} binding, however they have maintained the same coordinating atoms and comparable geometry to achieve similar selectivity. Interestingly, although the third type of Zn^{2+} binding sequence CysCysXXGlu is found mainly in plant Zn^{2+}-ATPases, examples of this can also be found in bacterial proteins (*Oscillatoria brevis* Q8L158, *Flavobacterium johnsoniae* Q1XX99, and *Shewanella putrefaciens* Q2ZQU0). However, in these, the carboxyl group is provided by an Asp residue rather than Glu in the eukaryote proteins.

HMA2 N-MBD mutagenesis and metal binding studies also showed that Cu^+ and Zn^{2+} are differentially coordinated during binding to this domain. Cys17, Cys18, and Glu21 are likely involved in Zn^{2+} binding, whereas only Cys17 and Glu21 coordinate Cu^+. This is in agreement with previous work showing that the CysXXCys coordinates Cu^+ in a linear

fashion (*23*, *60*), whereas Zn^{2+} appears tetrahedrically coordinated by two sulfydryl, a carboxyl, and an external group, possibly a H_2O molecule (*40*). Although HMA2 N-MBD coordinates nonsubstrate Cu^{+}, the presence of Glu residue probably increases its affinity for Zn^{2+}. A central importance has been given to the carboxyl group to confer selectivity to Zn^{2+}-ATPase N-MBDs (*39*, *40*). However, while the carboxyl group appears necessary for Zn^{2+} binding by the HMA2 CysCysXXGlu site, its role with bacterial CysXXCys has not been explored. In any case, it should be kept in mind that *in vivo* the selective binding of activating metals to these N-MBDs might not only be determined by the metal coordination but also by specific interaction of chaperones or other metal binding molecules.

Functional Role of N-MBD. In order to determine how the N-MBD affects the enzyme activity, we analyzed the metal dependent ATPase activity of the ΔN-HMA2 and HMA2 carrying mutations in the metal coordinating residues Cys17, Cys18, and Glu21. Both types of structural modifications resulted in ≈50% reduction in the enzymes V_{max} without significantly altering the metal dependence for activity. This is, the metal $k_{1/2}$ for activation or the relative V_{max} obtained in the presence of various metals (Zn^{2+}, Cd^{2+}, or Cu^{+}) did not change. Therefore, although the N-MBD is required for maximum enzyme turnover rate, it would not influence the metal binding to TMBDs and the resulting transport selectivity. The similar enzyme kinetics observed in ΔN-HMA2 and proteins carrying point mutations also suggest that the decrease in enzyme activity is dependent on the removal of the N-MBD metal binding capability rather than on nonspecific misfolding of the protein. This concept is further supported by high activities observed in proteins carrying mutations in Ser20 that do not affect the N-MBD metal binding.

Effects similar to those described for HMA2 lacking the N-MBD metal binding capabilities have been observed in studies of other P_{1B}-type ATPases including bacterial Zn^{2+}-ATPases (*31*−*34*, *58*, *59*, *67*). These data contribute to a hypothetical common mechanism of transport regulation via domain−domain interactions. Related to this, HMA2 C-MBD also regulates the enzyme turnover rate (*12*). Interestingly, truncation of both N-MBD and C-MBD results in a similar decrease in V_{max} when either of the domains is truncated, indicating that these domains might function in a coordinated manner; i.e., removal of either component leads to system disfunction (*12*).

In summary, HMA2 N-MBD appears as a metal binding regulatory domain that is required for maximum enzyme turnover rate. This domain selectively binds Zn^{2+} and Cd^{2+} by coordination through conserved Cys and Glu residues. These observations indicate that plant Zn^{2+}-ATPase N-MBDs bind the activating metal in a fashion similar to bacterial Zn^{2+}-ATPases, but using the distinct CysCysXXGlu sequence.

ACKNOWLEDGMENT

We thank Dr. C. Robert Matthews (University of Massachusetts Medical School, Worcester, MA) for enabling us to perform circular dichroism analysis of N-MBD. We also thank Don Pellegrino (Worcester Polytechnic Institute, Worcester, MA) for his kind help and assistance with AAS determinations.

REFERENCES

1. Argüello, J. M. (2003) Identification of ion selectivity determinants in heavy metal transport P1B-type ATPases, *J. Membr. Biol. 195*, 93−108.
2. Rensing, C., Ghosh, M., and Rosen, B. P. (1999) Families of soft-metal-ion transporting ATPases, *J. Bacteriol. 181*, 5891−5897.
3. Axelsen, K. B., and Palmgren, M. G. (1998) Evolution of substrate specificities in the P-type ATPase superfamily, *J. Mol. Evol. 46*, 84−101.
4. Williams, L. E., and Mills, R. F. (2005) P_{1B}-ATPases-an ancient family of transition metal pumps with diverse function in plants, *Trends Plant Sci. 10*, 491−502.
5. Lutsenko, S., and Petris, M. J. (2003) Function and regulation of the mammalian copper-transporting ATPases: insights from biochemical and cell biological approaches, *J. Membr. Biol. 192*, 1−12.
6. Bull, P. C., and Cox, D. V. (1994) Wilson disease and Menkes disease: new handles on heavy-metal transport, *Trends Genet. 10*, 246−252.
7. Hirayama, T., Kieber, J. J., Hirayama, N., Kogan, M., Guzman, P., Nourizadeh, S., Alonso, J. M., Dailey, W. P., Dancis, A., and Ecker, J. R. (1999) RESPONSIVE-TO-ANTAGONIST1, a Menkes/Wilson disease-related copper transporter, is required for ethylene signaling in Arabidopsis, *Cell 97*, 383−393.
8. Eren, E., and Argüello, J. M. (2004) Arabidopsis HMA2, a divalent heavy metal-transporting P_{1B}-type ATPase, is involved in cytoplasmic Zn^{+2} homeostasis, *Plant Physiol. 136*, 3712−3723.
9. Hussain, D., Haydon, M. J., Wang, Y., Wong, E., Sherson, S. M., Young, J., Camakaris, J., Harper., J. F., and Cobbett, C. S. (2004) P-type ATPase heavy metal transporters with roles in essential zinc homeostasis in arabidopsis, *Plant Cell 16*, 1327−1339.
10. Andres-Colas, N., Sancenon, V., Rodriguez-Navarro, S., Mayo, S., Thiele, D. J., Ecker, J. R., Puig, S., and Penarrubia, L. (2006) The Arabidopsis heavy metal P-type ATPase HMA5 interacts with metallochaperones and functions in copper detoxification of roots, *Plant J. 45*, 225−236.
11. Shikanai, T., Muller-Moule, P., Munekage, Y., Niyogi, K. K., and Pilon, M. (2003) PAA1, a P-type ATPase of Arabidopsis, functions in copper transport in chloroplasts, *Plant Cell 15*, 1333−1346.
12. Eren, E., Kennedy, D. C., Maroney, M. J., and Argüello, J. M. (2006) A novel regulatory metal binding domain is present in the C terminus of Arabidopsis Zn2+-ATPase HMA2, *J. Biol. Chem. 281*, 33881−33891.
13. Verret, F., Gravot, A., Auroy, P., Preveral, S., Frostier, C., Vavasseur, A., and Richaud, P. (2005) Heavy metal transport by AtHMA4 involves the N-terminal degenerated metal binding domain and the C-terminal His_{11} stretch, *FEBS Lett. 579*, 1515−1522.
14. Lutsenko, S., and Kaplan, J. H. (1995) Organization of P-type ATPases: significance of structural diversity, *Biochemistry 34*, 15607−15613.
15. Mandal, A. K., Yang, Y., Kertesz, T. M., and Argüello, J. M. (2004) Identification of the transmembrane metal binding site in Cu^{+}-transporting P1B-type ATPases, *J. Biol. Chem. 279*, 54802−54807.
16. Lowe, J., Vieyra, A., Catty, P., Guillain, F., Mintz, E., and Cuillel, M. (2004) A mutational study in the transmembrane domain of Ccc2p, the yeast Cu(I)-ATPase, shows different roles for each Cys-Pro-Cys cysteine, *J. Biol. Chem. 279*, 25986−25994.
17. Dutta, S. J., Liu, J., Hou, Z., and Mitra, B. (2006) Conserved aspartic acid 714 in transmembrane segment 8 of the ZntA subgroup of P1B-type ATPases is a metal-binding residue, *Biochemistry 45*, 5923−5931.
18. Wu, C.-C., Gardarin, A., Martel, A., Mintz, E., Guillain, F., and Catty, P. (2006) The cadmium transport Sites of CadA, the Cd2+-ATPase from *Listeria monocytogenes*, *J. Biol. Chem. 281*, 29533−29541.
19. Sazinsky, M. H., Mandal, A. K., Argüello, J. M., and Rosenzweig, A. C. (2006) Structure of the ATP binding domain from the Archaeoglobus fulgidus Cu+-ATPase, *J. Biol. Chem. 281*, 11161−11166.

20. Sazinsky, M. H., Agarwal, S., Argüello, J. M., and Rosenzweig, A. C. (2006) Structure of the actuator domain from the Archaeoglobus fulgidus Cu(+)-ATPase, *Biochemistry 45*, 9949−9955.
21. Arnesano, F., Banci, L., Bertini, I., Ciofi-Baffoni, S., Molteni, E., Huffman, D. L., and O'Halloran, T. V. (2002) Metallochaperones and metal-transporting ATPases: a comperative analysis of sequences and structures, *Genome Res. 12*, 255−271.
22. Banci, L., Bertini, I., Ciofi-Baffoni, S., Huffman, D. L., and O'Halloran, T. V. (2001) Solution structure of the yeast copper transporter domain Ccc2a in the Apo and Cu(I)-loaded States, *J. Biol. Chem. 276*, 8415−8426.
23. Gitschier, J., Moffat, B., Reilly, D., Wood, W. I., and Fairbrother, W. J. (1998) Solution structure of the fourth metal-binding domain from the Menkes copper-transporting ATPase, *Nat. Struct. Biol. 5*, 47−54.
24. Banci, L., Bertini, I., Del Conte, R., Markey, J., and Ruiz-Duenas, F. J. (2001) Copper trafficking: the solution structure of Bacillus subtilis CopZ, *Biochemistry 40*, 15660−15668.
25. Rosenzweig, A. C., Huffman, D. L., Hou, M. Y., Wernimont, A. K., Pufahl, R. A., and O'Halloran, T. V. (1999) Crystal structure of the Atx1 metallochaperone protein at 1.02 A resolution, *Structure 7*, 605−617.
26. DiDonato, M., Narindrasorasak, S., Forbes, J. R., Cox, D. W., and Sarkar, B. (1997) Expression, purification, and metal binding properties of the N-terminal domain from the Wilson disease putative copper-transporting ATPase (ATP7B), *J. Biol. Chem. 272*, 33279−33282.
27. Lutsenko, S., Petrukhin, K., Cooper, M. J., Gilliam, C. T., and Kaplan, J. H. (1997) N-terminal domains of human copper-transporting adenosine triphosphatases (the Wilson's and Menkes disease proteins) bind copper selectively in vivo and in vitro with stoichiometry of one copper per metal-binding repeat, *J. Biol. Chem. 272*, 18939−18944.
28. Huffman, D. L., and O'Halloran, T. V. (2000) Energetics of copper trafficking between the Atx1 metallochaperone and the intracellular copper transporter, Ccc2, *J. Biol. Chem. 275*, 18611−18614.
29. Wernimont, A. K., Huffman, D. L., Lamb, A. L., O'Halloran, T. V., and Rosenzweig, A. C. (2000) Structural basis for copper transfer by the metallochaperone for the Menkes/Wilson disease proteins, *Nat. Struct. Biol. 7*, 766−771.
30. Walker, J. M., Tsivkovskii, R., and Lutsenko, S. (2002) Metallochaperone Atox1 transfers copper to the NH2-terminal domain of the Wilson's disease protein and regulates its catalytic activity, *J. Biol. Chem. 277*, 27953−27959.
31. Voskoboinik, I., Strausak, D., Greenough, M., Brooks, H., Petris, M., Smith, S., Mercer, J. F., and Camakaris, J. (1999) Functional analysis of the N-terminal CXXC metal-binding motifs in the human Menkes copper-transporting P-type ATPase expressed in cultured mammalian cells, *J. Biol. Chem. 274*, 22008−22012.
32. Fan, B., and Rosen, B. P. (2002) Biochemical characterization of CopA, the *Escherichia coli* Cu(I)-translocating P-type ATPase, *J. Biol. Chem. 277*, 46987−46992.
33. Mandal, A. K., and Argüello, J. M. (2003) Functional roles of metal binding domains of the *Archaeglobus fulgidus* Cu^{+}-ATPase CopA, *Biochemistry 42*, 11040−11047.
34. Mana-Capelli, S., Mandal, A. K., and Argüello, J. M. (2003) *Archaeoglobus fulgidus* CopB is a thermophilic Cu^{2+}-ATPase: Functional role of its histidine-rich N-terminal metal binding domain, *J. Biol. Chem. 278*, 40534−40541.
35. Tsivkovskii, R., MacArthurs, B., and Lutsenko, S. (2001) The Lys-(1010)-Lys(1325) fragment of the Wilson's disease protein binds nucleotides and interacts with the N-terminal domain of this protein in a copper-dependent manner, *J. Biol. Chem. 276*, 2234−2242.
36. Petris, M. J., Mercer, J. F., Culvenor, J. G., Lockhart, P., Gleeson, P. A., and Camakaris, J. (1996) Ligand-regulated transport of the Menkes copper P-type ATPase efflux pump from the Golgi apparatus to the plasma membrane: a novel mechanism of regulated trafficking, *EMBO J. 15*, 6084−6095.
37. Schaefer, M., Hopkins, R. G., Failla, M. L., and Gitlin, J. D. (1999) Hepatocyte-specific localization and copper-dependent trafficking of the Wilson's disease protein in the liver, *Am. J. Physiol. 276*, G639−G646.
38. Mills, R. F., Francini, A., Ferreira da Rocha, P. S. C., Baccarani, P. J., Aylett, M., Krijger, G. C., and Williams, L. E. (2005) The plant P_{1B}-type ATPase AtHMA4 transports Zn and Cd and plays a role in detoxification of transition metals supplied at elevated levels, *FEBS Lett. 579*, 783−791.
39. Banci, L., Bertini, I., Ciofi-Baffoni, S., Su, X.-C., Miras, R., Bal, N., Mintz, E., Catty, P., Shokes, J. E., and Scott, R. A. (2006) Structural basis for metal binding specificity: the N-terminal cadmium binding domain of the P1-type ATPase CadA, *J. Mol. Biol. 356*, 638−650.
40. Banci, L., Bertini, I., Ciofi-Baffoni, S., Finney, L. A., Outten, C. E., and O'Halloran, T. V. (2002) A new Zinc-protein coordination site in intracellular metal trafficking: solution structure of the apo and Zn(II) forms of ZntA (46-118), *J. Mol. Biol. 323*, 883−897.
41. Bradford, M. M. (1976) A rapid and sensitive method for the quantitation of microgram quantities of protein utilizing the principle of protein-dye binding, *Anal. Biochem. 72*, 248−254.
42. Laemmli, U. K. (1970) Cleavage of structural proteins during the assembly of the head of bacteriophage T4, *Nature 227*, 680−685.
43. Lanzetta, P. A., Alvarez, L. J., Reinach, P. S., and Candia, O. A. (1979) An improved assay for nanomole amounts of inorganic phosphate, *Anal. Biochem. 100*, 95−97.
44. Liu, J., Stemmler, A. J., Fatima, J., and Mitra, B. (2005) Metal-binding characteristics of the amino-terminal domain of ZntA: binding of lead is different compared to cadmium and zinc, *Biochemistry 44*, 5159−5167.
45. Guo, J., and Giedroc, D. P. (1997) Zinc site redesign in T4 gene 32 protein: structure and stability of Co(II) complexes formed by wild-type and metal ligand substitution mutants, *Biochemistry 36*, 730−742.
46. Lobley, A., Whitmore, L., and Wallace, B. A. (2002) DICHROWEB: an intreactive website for the analysis of protein secondary structure from circular dichroism spectra, *Bioinformatics 18*, 211−212.
47. Whitmore, L., and Wallace, B. A. (2004) DICHROWEB, an online server for protein secondary structure analyses from circular dichroism spectroscopic data, *Nucleic Acids Res. 32*, W668−W673.
48. Andrade, M. A., Chacón, P., Merelo, J. J., and Morán, F. (1993) Evaluation of secondary structure of proteins from UV circular dichroism using an unsupervised learning neural network, *Protein Eng. 6*, 383−390.
49. Thompson, J. D., Higgins, D. G., and Gibson, T. J. (1994) CLUSTAL W: improving the sensitivity of progressive multiple sequence alignment through sequence weighting, position-specific gap penalties and weight matrix choice, *Nucleic Acids Res. 22*, 4673−4680.
50. Page, R. (1996) TREEVIEW: an application to display phylogenetic trees on personal computers, *Appl. Biosci. 12*, 357−358.
51. Pearson, W. R. (1990) Rapid and sensitive sequence comparison with FASTAP and FASTA, *Methods Enzymol. 183*, 63−98.
52. Guex, N., and Peitsch, M. C. (1997) SWISS-MODEL and the Swiss-Pdb Viewer: An environment for comparative protein modelling, *Electrophoresis 18*, 2714−2723.
53. Schwede, T., Kopp, J., Guex, N., and Peitsch, M. C. (2003) SWISS-MODEL: an automated protein homology-modeling server, *Nucleic Acids Res. 31*, 3381−3385.
54. Vriend, G. (1990) WHAT IF: A molecular modelling and drug design program, *J. Mol. Graphics 8*, 52−56.
55. Hooft, R., Sander, C., Vriend, G., and Abola, E. (1996) Errors in protein structures, *Nature 381*, 272.
56. Mandal, A. K., Cheung, W. D., and Argüello, J. M. (2002) Characterization of a thermophilic P-type Ag+/Cu+-ATPase from the extremophile Archaeoglobus fulgidus, *J. Biol. Chem. 277*, 7201−7208.
57. Walkup, G. K., and Imperiali, B. (1997) Fluorescent chemosensors for divalent zinc based on zinc finger domains. Enhanced oxidative stability, metal binding affinity, and structural and functional characterization, *J. Am. Chem. Soc. 119*, 3443−3450.
58. Bal, N., Mintz, E., Guillain, F., and Catty, P. (2001) A possible regulatory role for the metal metal-binding domain of CadA, the *Listeria monocytogenes* Cd^{2+}-ATPase, *FEBS Lett. 506*, 249−252.
59. Mitra, B., and Sharma, R. (2001) The cysteine-rich amino-terminal domain of ZntA, a Pb(II)/Zn(II)/Cd(II)-translocating ATPase from *Escherichia coli*, is not essential for its function, *Biochemistry 40*, 7694−7699.

60. Ralle, M., Lutsenko, S., and Blackburn, N. J. (2003) The Menkes disease protein binds copper via novel 2-coordinate Cu^{+}-cysteinates in the N-terminal domain, *J. Biol. Chem. 278*, 23163−23170.
61. Anastassopoulou, I., Banci, L., Bertini, I., Cantini, F., Katsari, E., and Rosato, A. (2004) Solution structure of the apo and copper-(I)-loaded human metallochaperone HAH1, *Biochemistry 43*, 13046−13053.
62. DiDonato, M., Zhang, J., Que, L., Jr., and Sarkar, B. (2002) Zinc binding to the NH_2-terminal domain of the Wilson disease copper-transporting ATPase: implications for in vivo metal ion-mediated regulation of ATPase activity, *J. Biol. Chem. 277*, 13409−13414.
63. Xiao, Z., Loughlin, F., George, G. N., Howlett, G. J., and Wedd, A. G. (2004) C-terminal domain of the membrane copper transporter Ctr1 from Saccharomyces cerevisiae binds four Cu(I) as a cuprous-thiolate polynuclear cluster: sub-femtomolar Cu(I) affinity of three proteins involved in copper trafficking, *J. Am. Chem. Soc. 126*, 3081−3090.
64. Urvoas, A., Moutiez, M., Estienne, C., Couprie, J., Mintz, E., and Le Clainche, L. (2004) Metal-binding stoichiometry and selectivity of the copper chaperone CopZ from *Enterococcus hirae*, *Eur. J. Biochem. 271*, 993−1003.
65. DeSilva, T. M., Veglia, G., and Opella, S. J. (2005) Solution structures of the reduced and Cu(I) bound forms of the first metal binding sequence of ATP7A associated with Menkes disease, *Proteins 61*, 1038−1049.
66. Jensen, P. Y., Bonander, N., Máller, L. B., and Farver, O. (1999) Cooperative binding of copper(I) to the metal binding domains in Menkes disease protein, *Biochim. Biophys. Acta 1434*, 103−113.
67. Voskoboinik, I., Mar, J., Strausak, D., and Camakaris, J. (2001) The regulation of catalytic activity of the Menkes copper-translocating P-type ATPase: Role of high affinity copper-binding sites, *J. Biol. Chem. 276*, 28620−28627.

BI7001345